

# Supporting Information

## Engineering the Oxidative Potency of Non-Heme Iron(IV) Oxo Complexes in Water for C–H Oxidation by a cis Donor and Variation of the Second Coordination Sphere

Christina Wegeberg,<sup>a,b,†</sup> Mathias L. Skavenborg,<sup>a,c</sup> Andrea Liberato,<sup>d</sup> James N. McPherson,<sup>a</sup> Wesley R. Browne,<sup>b</sup> Erik D. Hedegård<sup>e</sup> and Christine J. McKenzie<sup>a,\*</sup>

<sup>a</sup>Department of Physics, Chemistry and Pharmacy, University of Southern Denmark, Campusvej 55, 5230 Odense M (Denmark). Email: [mckenzie@sdu.dk](mailto:mckenzie@sdu.dk)

<sup>b</sup>Molecular Inorganic Chemistry, Stratingh Institute for Chemistry, University of Groningen, Nijenborgh 4, 9747 AG Groningen (The Netherlands)

<sup>c</sup>Water Research Centre, School of Civil and Environmental Engineering, University of New South Wales, Sydney, NSW (Australia)

<sup>d</sup>Universidad de Cádiz, Facultad de Ciencias, Departamento de Ciencia de los Materiales e Ingeniería Metalúrgica y Química Inorgánica, Puerto Real, Cádiz 11510 (Spain)

<sup>e</sup>Division of Theoretical Chemistry, Lund University, Naturvetarvägen 14, 221 00 Lund (Sweden)

<sup>†</sup> Present address: Department of Chemistry, University of Basel, St. Johannis-Ring 19, 4056 Basel (Switzerland)

	Instrumentation and Methods	S2
	Computational Details	S3
	Materials and Preparation	S4
<b>Tables S1 – S3</b>	Crystallographic data for [VO(tpen)](ClO <sub>4</sub> ) <sub>2</sub> and [VO(tpenOH)](PF <sub>6</sub> ) <sub>2</sub>	S5
<b>Table S4</b>	DFT calculated relative Gibbs free energies of tpenO-based iron(IV)oxo complexes	S7
<b>Table S5</b>	DFT calculated relative Gibbs free energies of tpena-based iron(IV)oxo complexes	S8
<b>Figure S1</b>	NMR study of [Fe <sub>2</sub> O(Htpena) <sub>2</sub> ](ClO <sub>4</sub> ) <sub>4</sub> dissolved in D <sub>2</sub> O with NaOCl addition	S9
<b>Figure S2</b>	Raman spectra of iron(IV)oxo complexes	S10
<b>Figures S3 –S9</b>	Reactivity Studies towards C-H bonds	S11
<b>Figure S10</b>	ESI-MS spectra series of [FeCl(tpenOH)] <sup>+</sup> undergoing oxidation	S17
	References	S18

## Instrumentation and Methods

All experiments were carried out at room temperature. UV/Vis spectra were recorded in 1 cm quartz cuvettes on an Agilent 8453 spectrophotometer. IR spectra were recorded in the solid state (FT-ATR diamond anvil) on a Spectrum 65 FT-IR spectrometer (PerkinElmer). Raman spectra were recorded at 785 nm with one of the following: a RamanStation (Perkin Elmer) equipped with a BX51 upright microscope (80 mW at sample), a RamanFlex (Perkin Elmer) equipped with an Inphotonics industrial probe or a free space laser (75 mW, Ondax, with a 785 nm laser line clean up filter) and collected in back scattering ( $180^\circ$ ) mode with a Semrock dichroic beamsplitter and a 25 mm diameter/7.5 cm planoconvex lens to focus the laser on the sample and collect the Raman scattering. The Raman scattering was passed through a long pass filter (Semrock) and focused into a Shamrock300 spectrograph (ANDOR technology) and dispersed onto a iDUS-420-BUEX2 CCD camera. Spectra were calibrated with MeCN/toluene (50:50 v/v).  $^1\text{H}$  NMR spectra were recorded on a Bruker Avance III 400 spectrometer at ambient temperature. Chemical shifts are denoted relative to the residual solvent peak of  $\text{D}_2\text{O}$  ( $\delta = 4.79$  ppm). ESI-MS spectra were performed on a nanospray Bruker micro-OTOF-Q II spectrometer in positive-ionization mode. The aqueous iron solutions (1 mg/1mL) were diluted to 10  $\mu\text{g}/\text{mL}$  with MeCN before injection. The software mMass (version 5.4.1.0) was employed for the visualization and handling of the spectra. Elementary analysis (C, H, N) was performed on a FlashEA 1112. Reactivity studies were performed on 1.2 mL aqueous solutions of 1.5 mM [Fe] solutions at 22  $^\circ\text{C}$  with vigorous stirring to ensure proper mixing of the aqueous solutions and the miscible substrates. The pseudo-first order decay curves were obtained by monitoring the decrease in absorbance of the iron(IV)oxo species,  $\lambda_{\text{max}}$ , over time upon different concentrations of substrate were added (in the range of 0.1 M – 1.0 M). These profiles were fitted with an exponential decay function using OriginPro 9.0 to obtain the rate constants,  $k_{\text{obs}}$ .  $k_{\text{obs}}$  values were plotted against the concentrations of substrate, and their slopes (linear regression) represent the second-order rate constants ( $k_2$ ). Product analysis upon complete decay of  $\lambda_{\text{max}}$  monitored by UV/Vis spectroscopy was performed on a Hewlett Packard 6890 Series gas chromatograph system with a flame ionization detector. X-ray crystal diffraction data for  $[\text{VO}(\text{tpen})](\text{ClO}_4)_2$  and  $[\text{V}^{\text{IV}}\text{O}(\text{tpenOH})](\text{PF}_6)_2$  were collected at 100(2)K on a Synergy, Dualflex, AtlasS2 diffractometer using  $\text{CuK}\alpha$  radiation ( $\lambda = 1.54184 \text{ \AA}$ ) and the CrysAlis PRO 1.171.38.43 suite. The structures were solved by dual space methods (SHELXT) and refined on  $F^2$  using all the reflections (SHELXL-2016/2018). For  $[\text{VO}(\text{tpen})](\text{ClO}_4)_2$  all the non-hydrogen atoms were refined using anisotropic atomic displacement parameters and hydrogen atoms were inserted at calculated positions using a riding model. For the structure of  $[\text{V}^{\text{IV}}\text{O}(\text{tpenOH})](\text{PF}_6)_2$  there is significant disorder of one of the  $\text{PF}_6^-$  counter anions (P2, F7, F8, F9, F10, F11 and F12) and the ethanol arm (C21, C22, O2). Thus the atoms were modelled over two positions. All other non-hydrogen atoms were refined using anisotropic atomic displacement parameters, and hydrogen atoms were inserted at calculated positions using a riding model, including the alcohol H atom. CCDC 1971388 and 2017382 contain the supplementary crystallographic data for this paper.

## Computational Details

All calculations were carried out with the Gaussian 16 program<sup>1</sup> employing density functional theory (DFT) in the unrestricted Kohn-Sham formulation. We employed the generalized gradient approximation (GGA) hybrid B3LYP<sup>2-4</sup> functional and the (non-hybrid) *meta*-GGA functional TPSS.<sup>5</sup> All calculations were done with the def2-TZVPP basis set.<sup>6,7</sup> All energies are reported from optimized structures at the same level of theory. In addition, harmonic frequencies were calculated to obtain thermochemical corrections (using a temperature of 25° C). All calculations were carried out with polarizable continuum model (PCM)<sup>8</sup> to mimic the water solvent (using default input parameters).

The hybrid functional B3LYP is known to be biased towards high-spin states, and the non-hybrid functional TPSS to be bias towards low-spin states.<sup>9</sup> The two functionals provide large differences in spin state splittings, but in most cases agrees on that the  $S = 1$  state is the most stable (table S4 and S5). The only exception is  $[\text{Fe}^{\text{IV}}\text{O}(\text{HtpenO})]^{2+}$ , where B3LYP yields  $S = 2$  and TPSS yields the  $S = 1$  spin state as most stable. In the case of  $[\text{Fe}^{\text{IV}}\text{O}(\text{Htpena})]^{2+}$  the  $S = 1$  state calculated is in agreement with previously obtained Mössbauer parameters ( $\delta = 0.00 \text{ cm}^{-1}$ ,  $\Delta E_Q = 0.90 \text{ cm}^{-1}$ ).<sup>10</sup>

## Materials and Preparation

The complexes  $[\text{FeCl}(\text{tpenOH})](\text{PF}_6)$ ,  $[\text{FeCl}(\text{ettpen})](\text{PF}_6)$ ,  $[\text{Fe}_2\text{O}(\text{Htpena})](\text{ClO}_4)_4$ ,  $[\text{FeCl}(\text{bztpen})](\text{PF}_6)$ ,  $[\text{Fe}(\text{tpen})](\text{PF}_6)_2$ , and  $[\text{FeCl}(\text{metpen})](\text{PF}_6)$  were synthesized as previously reported.<sup>11–15</sup> CAN, NaClO (14 %, aq.) and substrates were purchased from commercial suppliers and used without further purification. The aqueous solutions were either prepared from demineralised water or  $^{18}\text{O}$ - $\text{H}_2\text{O}$  (supplied by Rotem Industries Ltd.).

*Perchlorate salts of metal complexes are potentially explosive and should be handled with caution in small quantities.*

### $[\text{V}^{\text{IV}}\text{O}(\text{tpen})](\text{ClO}_4)_2$

$\text{VO}(\text{ClO}_4)_2$  (29.5 mg, 0.115 mmol) was dissolved in MeOH:MeCN (2:1, 3 ml) by heating under reflux. tpen (51.4 mg, 0.121 mmol) and  $\text{NaClO}_4$  (34 mg, 0.278 mmol) dissolved in MeOH (2 ml) were added, and the reaction mixture was refluxed for additional 5 minutes. Upon slow cooling a blue crystalline material precipitated, which was isolated by vacuum filtration and washed with MeOH to afford 41 mg (53 %) of  $[\text{VO}(\text{tpen})](\text{ClO}_4)_2$ . Anal. Calcd. (%) for  $\text{C}_{26}\text{H}_{28}\text{Cl}_2\text{N}_6\text{O}_9\text{V}$ ; C: 45.23, H: 4.09, N: 12.17. Found C: 44.90, H: 4.40, N: 11.90. ESI-MS (pos. mode, MeCN),  $m/z$  590.1282 (590.1244, 3%,  $[\text{V}^{\text{IV}}\text{O}(\text{tpen}) + \text{ClO}_4]^+$ ), 507.1713, (507.1746, 100%,  $[\text{V}^{\text{V}}(\text{O})(\text{O})(\text{tpen})]^+$ ), 245.5891 (245.5877, 22%,  $[\text{V}^{\text{IV}}\text{O}(\text{tpen})]^{2+}$ ). IR (FT-ATR diamond anvil)  $\nu_{\text{V=O}}$  986  $\text{cm}^{-1}$ .

### $[\text{V}^{\text{IV}}\text{O}(\text{tpenOH})](\text{PF}_6)_2$

$\text{VOSO}_4 \cdot 5\text{H}_2\text{O}$  (71 mg, 0.281 mmol), tpenOH (104 mg, 0.276 mmol) and  $\text{Et}_3\text{N}$  (67 mg, 37  $\mu\text{L}$ , 0.265 mmol) dissolved in  $\text{H}_2\text{O}$  (2.5 mL) were heated to boiling point.  $\text{KPF}_6$  (131 mg, 0.712 mmol) dissolved in MeOH (2 mL) was added to the hot solution and the reaction mixture was slowly cooled to r.t. to afford  $[\text{V}^{\text{IV}}\text{O}(\text{tpenOH})](\text{PF}_6)_2$  as green crystals suitable for x-ray crystallography. Yield: 186 mg (0.253 mmol, 92%). ESI-MS (pos. mode, MeOH),  $m/z$  443.1525 (443.1526, 100%,  $[\text{V}^{\text{IV}}\text{O}(\text{tpenO})]^+$ ). IR (FT-ATR diamond anvil)  $\nu_{\text{V=O}}$  986  $\text{cm}^{-1}$ .

## Generation of Iron(IV)oxo Species

The iron(IV)oxo complexes were generated from their iron(II)/iron(III) precursors when dissolved in water with addition of 3 eq. of either CAN or NaClO at rt. The formation of green-blue chromophores was monitored by following the increase in  $\lambda_{\text{max}}$  around 720 nm  $\pm$  10 nm in the UV/Vis spectrum. The ambient pH of the iron(II)/iron(III) solutions are 5. The pH of the solutions decreases to 2 upon addition of CAN (3 eq.) and increases to 7 upon addition of NaOCl (3 eq.). The lifetimes of all complexes are lowered when they are generated using ClO<sup>-</sup> compared to CAN.

**Table S1.** Crystallographic data for [VO(tpen)](ClO<sub>4</sub>)<sub>2</sub> and [VO(tpenOH)](PF<sub>6</sub>)<sub>2</sub>

Complex	[VO(tpen)](ClO <sub>4</sub> ) <sub>2</sub>	[VO(tpenOH)](PF <sub>6</sub> ) <sub>2</sub>
Empirical formula	C <sub>26</sub> H <sub>28</sub> Cl <sub>2</sub> N <sub>6</sub> O <sub>9</sub> V	
Formula weight (g/mol)	690.38	734.36
Temperature (K)	100(2)	100(2)
Crystal system	Triclinic	Monoclinic
Space group	<i>P</i> -1	<i>P</i> 2 <sub>1</sub> / <i>n</i>
<i>a</i> , <i>b</i> , <i>c</i> (Å)	9.3995(3), 10.6655(3), 14.3220(4)	10.0617 (1), 21.2223 (1), 12.9466 (1)
$\alpha$ , $\beta$ , $\gamma$ (°)	92.544(2), 95.375(2), 100.541(3)	90, 90.121 (1), 90
Volume (Å <sup>3</sup> )	1402.57(7)	2764.51 (4)
<i>Z</i>	2	4
Radiation type	Cu K $\alpha$	Cu K $\alpha$
Calculated density (g cm <sup>-3</sup> )	1.635	1.764
Abs. coefficient (mm <sup>-1</sup> )	5.29	5.17
<i>F</i> (000)	710	1484
Crystal size (mm)	0.15 × 0.06 × 0.02	0.17 × 0.10 × 0.06
Colour	Blue	Green
Habit	Needle	Irregular
$\theta_{\min}$ , $\theta_{\max}$ (°)	4.2, 76.6	4.0, 66.6
Index range	-11 ≤ <i>h</i> ≤ 9, -13 ≤ <i>k</i> ≤ 13, -17 ≤ <i>l</i> ≤ 15	-11 ≤ <i>h</i> ≤ 11, -25 ≤ <i>k</i> ≤ 25, -15 ≤ <i>l</i> ≤ 15
Refns. collected / unique / with <i>I</i> > 2 $\sigma$ ( <i>I</i> )	11413 / 5674 / 5337	94011 / 4871 / 4710
<i>R</i> <sub>int</sub>	0.020	0.040
Data / restraints / parameters	5674 / 0 / 397	4871 / 574 / 463
GOOF on <i>F</i> <sup>2</sup>	1.04	1.03
Final <i>R</i> <sub>1</sub> ( <i>F</i> ) <sup>a</sup> / <i>wR</i> <sub>2</sub> ( <i>F</i> <sup>2</sup> ) <sup>b</sup> ( <i>I</i> > 2 $\sigma$ ( <i>I</i> ))	0.033 / 0.0884	0.071 / 0.185
<i>R</i> <sub>1</sub> <sup>a</sup> / <i>wR</i> <sub>2</sub> ( <i>F</i> <sup>2</sup> ) <sup>b</sup> (all data)	0.036 / 0.0903	0.072 / 0.186
Largest diff. peak / hole (e Å <sup>-3</sup> )	0.69, -0.42	1.49, -0.92

<sup>a</sup>  $R_1 = \sum ||F_{\text{obs}}| - |F_{\text{calc}}|| / \sum |F_{\text{obs}}|$ . <sup>b</sup>  $wR_2(F^2) = \{ \sum [w (F_{\text{obs}}^2 - F_{\text{calc}}^2)^2] / \sum [w (F_{\text{obs}}^2)^2] \}^{1/2}$ .

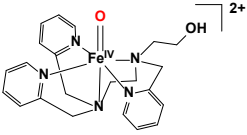
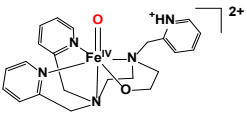
**Table S2. Selected bond distances and angles in [VO(tpen)](ClO<sub>4</sub>)<sub>2</sub>**

V1—O1	1.5943 (13)	O1—V1—N1	96.24 (6)
V1—N1	2.0999 (15)	O1—V1—N2	102.76 (7)
V1—N2	2.0842 (15)	O1—V1—N3	173.25 (6)
V1—N3	2.2834 (15)	O1—V1—N4	98.31 (6)
V1—N4	2.1122 (15)	O1—V1—N5	102.31 (6)
V1—N5	2.1553 (15)		

**Table S3. Selected bond distances and angles in [VO(tpenOH)](PF<sub>6</sub>)<sub>2</sub>**

V1—O1	1.591 (3)	O1—V1—N1	95.32 (15)
V1—N1	2.106 (4)	O1—V1—N2	101.34 (16)
V1—N2	2.092 (4)	O1—V1—N3	171.59 (15)
V1—N3	2.267 (4)	O1—V1—N4	99.81 (16)
V1—N4	2.118 (4)	O1—V1—N5	101.80 (16)
V1—N5	2.138 (4)		

**Table S4:** Calculation of the stabilities of isomers of the Fe(IV)oxo complex of tpenOH/HtpenO. DFT calculated relative Gibbs free energies in kJ/mol. Both  $S = 1$  (T) and  $S = 2$  (Q) are have been calculated  $\Delta G_{Q-T}$  are given in parentheses).  $\Delta E_{Q-T}$  denotes the electronic spin-state splitting (including ZPVE) in kJ/mol. Fe=O is stretch frequencies in  $\text{cm}^{-1}$  (for  $S = 1$  with the  $S = 2$  in parentheses). The stretches with largest displacements of Fe and O atoms are underlined.

Ligand	Func.	Most stable $S$	$\Delta E_{Q-T}$	$\Delta G$ ( $\Delta G_{Q-T}$ )	$\nu$ (Fe=O)	Structure
tpenOH	TPSS	1	81.6	0.0 (74.1)	<u>849</u> , <u>869</u> ( <u>878</u> )	
tpenOH	B3LYP	1	17.0	0.0 (9.2)	876, <u>906</u> ( <u>926</u> )	
HtpenO	TPSS	1	53.7	52.9 (45.9)	<u>835</u> , <u>837</u> ( <u>849</u> , <u>867</u> )	
HtpenO	B3LYP	2	0.2	53.6 (−3.9)	<u>866</u> , <u>884</u> ( <u>888</u> )	

**Table S5:** Calculation of the stabilities of isomers of the Fe(IV)oxo complex of tpena/Htpena/tpenaH. DFT calculated relative Gibbs free energies in kJ/mol. Both  $S = 1$  (T) and  $S = 2$  (Q) are have been calculated ( $\Delta G_{Q-T}$  are given in parentheses).  $\Delta E_{Q-T}$  denotes the electronic spin-state splitting (including ZPVE) in kJ/mol. The stretch frequencies of Fe=O are given in  $\text{cm}^{-1}$  (for  $S = 1$  with  $S = 2$  in parentheses). The stretches with largest displacements of Fe and O atoms are underlined.

Ligand	Functional	Most stable $S$	$\Delta E_{Q-T}$	$\Delta G$ ( $\Delta G_{Q-T}$ )	$\nu$ (Fe=O)	Structure
tpenaH	TPSS	1	70.8	0 (62.6)	847, <u>866</u> , 874 ( <u>873</u> )	
tpenaH	B3LYP	1	17.0	0 (9.2)	885, <u>907</u> (902, 921, 950)	
tpena	TPSS	1	73.9	0 (64.9)	847, <u>864</u> , 870 ( <u>872</u> )	
tpena	B3LYP	1	19.8	0 (12.4)	876, <u>904</u> (902, 916, 951)	
Htpena	TPSS	1	59.8	18.4 (54.5)	<u>854</u> , <u>871</u> (864, 891)	
Htpena	B3LYP	1	6.6	20.1 (2.4)	881, <u>907</u> (893, 923)	
tpena	TPSS	1	65.2	-23.1 (58.0)	<u>858</u> , <u>868</u> (864, 890)	
tpena	B3LYP	1	11.1	-23.9 (4.7)	<u>905</u> (894, 924)	
trans-Htpena	TPSS	1	39.1	46.5 (32.6)	<u>845</u> ( <u>860</u> )	
trans-Htpena	B3LYP	2	-15.0	30.9 (-21.3)	<u>891</u> ( <u>907</u> )	
trans-tpenaH	TPSS	1	25.7	67.8 (23.7)	831, <u>838</u> , 840, 853 ( <u>861</u> )	
trans-tpenaH	B3LYP	2	-23.6	50.3 (-27.7)	873, <u>887</u> ( <u>907</u> )	

The energy differences between the tpena isomers are generally smaller than for the corresponding tpenOH complex; only 20.1 kJ/mol (B3LYP) or 18.4 kJ/mol (TPSS) between  $[\text{Fe}^{\text{IV}}\text{O}(\text{Htpena})]^{2+}$  and  $[\text{Fe}^{\text{IV}}\text{O}(\text{tpenaH})]^{2+}$ , with the fully N coordinated  $[\text{Fe}^{\text{IV}}\text{O}(\text{tpenaH})]^{2+}$  being most stable. For the deprotonated variant both functionals predict that the O coordinated structure is the most stable, but the energy difference is again small (23–24 kJ/mol). These results indicate that in contrast to the tpenOH complexes, both isomers can exist in solution. The additional DFT calculations for isomers of  $[\text{Fe}^{\text{IV}}\text{O}(\text{tpenaH})]^{2+}$  and  $[\text{Fe}^{\text{IV}}\text{O}(\text{Htpena})]^{2+}$  where the *trans* donor to the Fe=O moiety was changed from a tertiary amine to either a pyridyl or the carboxylate showed that the *trans*-tertiary amine always comes out as most stable (by 50–68 kJ/mol compared to *trans*-pyridine and 31–46 kJ/mol compared to *trans*-carboxy).



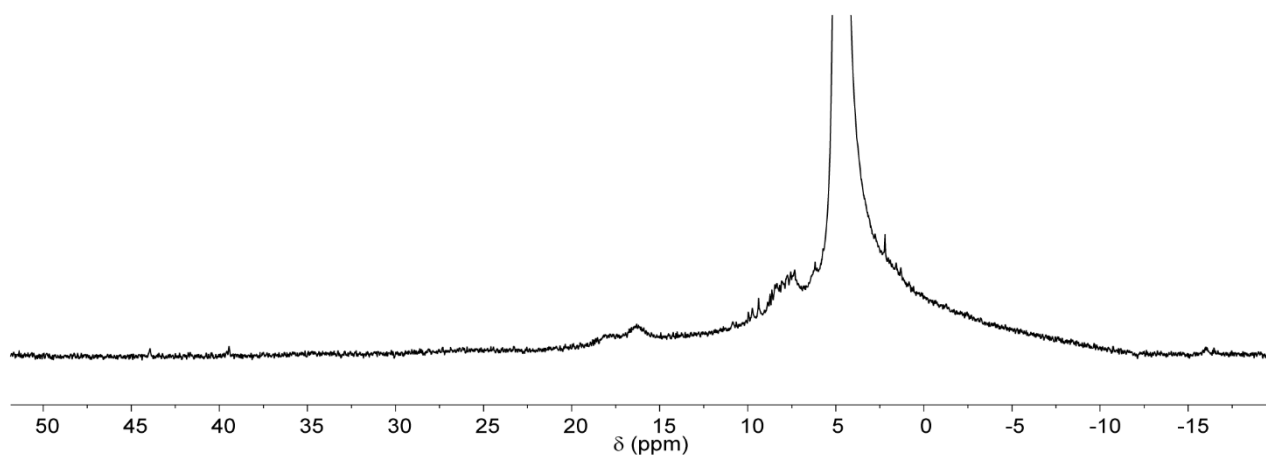


**Figure S1.**  $^1\text{H}$ -NMR (400 MHz) from 50 ppm to - 20 ppm of  $[\text{Fe}_2\text{O}(\text{Htpena})_2](\text{ClO}_4)_4$  dissolved in  $\text{D}_2\text{O}$  (1 mM) which has been oxidized with  $\text{NaClO}$  (6 eq.). The spectrum was acquired 30 minutes after  $\text{NaClO}$  addition.

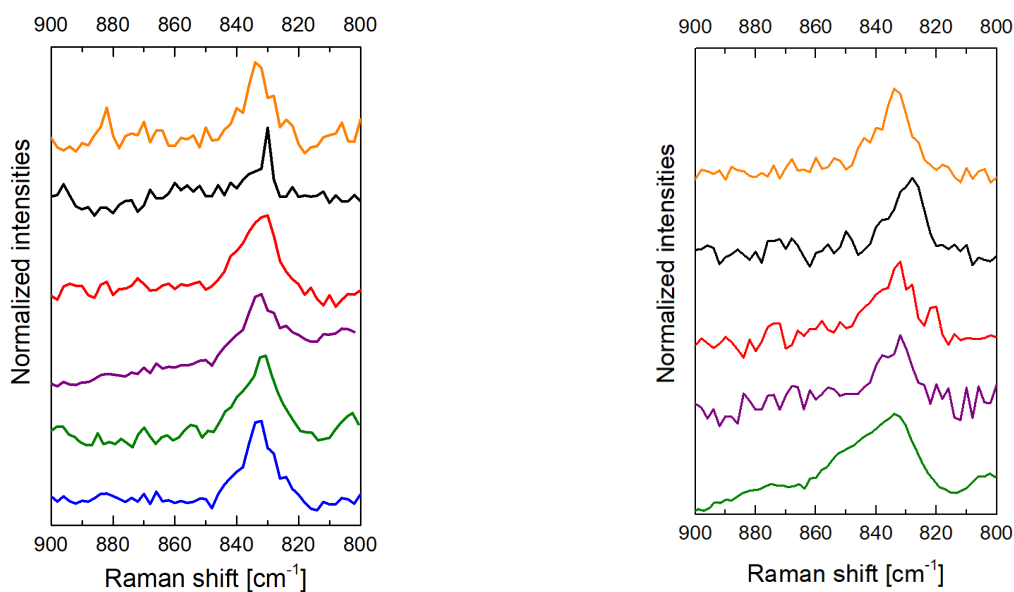


**Figure S2.** Raman spectra of  $[\text{Fe}^{\text{IV}}=\text{O}(\text{HtpenO})]^{2+}$  (blue,  $\lambda_{\text{max}}$  723 nm),  $[\text{Fe}^{\text{IV}}=\text{O}(\text{Htpena})]^{2+}$  (green,  $\lambda_{\text{max}}$  730 nm),  $[\text{Fe}^{\text{IV}}=\text{O}(\text{tpen})]^{2+}$  (purple,  $\lambda_{\text{max}}$  712 nm),  $[\text{Fe}^{\text{IV}}=\text{O}(\text{metpen})]^{2+}$  (red,  $\lambda_{\text{max}}$  714 nm),  $[\text{Fe}^{\text{IV}}=\text{O}(\text{bztpen})]^{2+}$  (black,  $\lambda_{\text{max}}$  722 nm) and  $[\text{Fe}^{\text{IV}}=\text{O}(\text{ettpen})]^{2+}$  (orange,  $\lambda_{\text{max}}$  718 nm) generated in  $\text{H}_2\text{O}$  from either 3 eq. CAN (left) or 3 eq.  $\text{NaOCl}$  (right) ( $[\text{Fe}] = 4$  mM,  $\lambda_{\text{exc}} = 785$  nm, rt).

## Reactivity Studies towards C-H Bonds

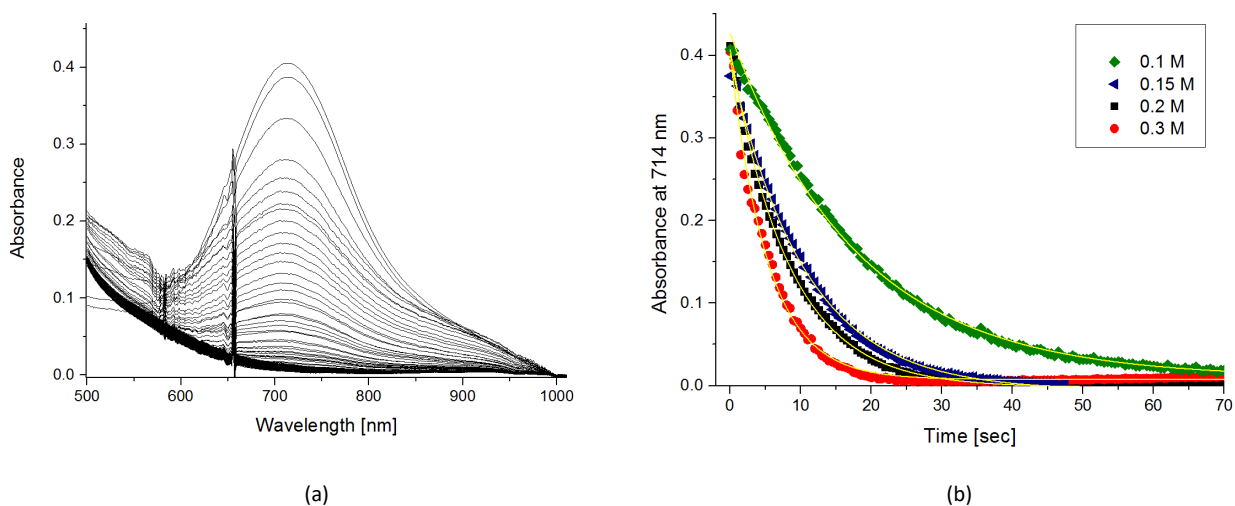


**Figure S3.** (a) Time-dependent UV/Vis of the decay of aqueous  $[\text{Fe}^{\text{IV}}\text{O}(\text{metpen})]^{2+}$  upon addition of benzyl alcohol and (b) time-trace of  $\lambda_{\text{max}}$  at 714 nm upon addition of four different concentrations of benzyl alcohol. The absorption-time decay profile is fitted to an exponential function shown in yellow to obtain  $k_{\text{obs}}$  values. pH = 2 (3. eq CAN),  $[\text{Fe}] = 1.5$  mM. Analogues analysis has been done for all complexes and substrates summarized in table 1 and table 2 in the manuscript.

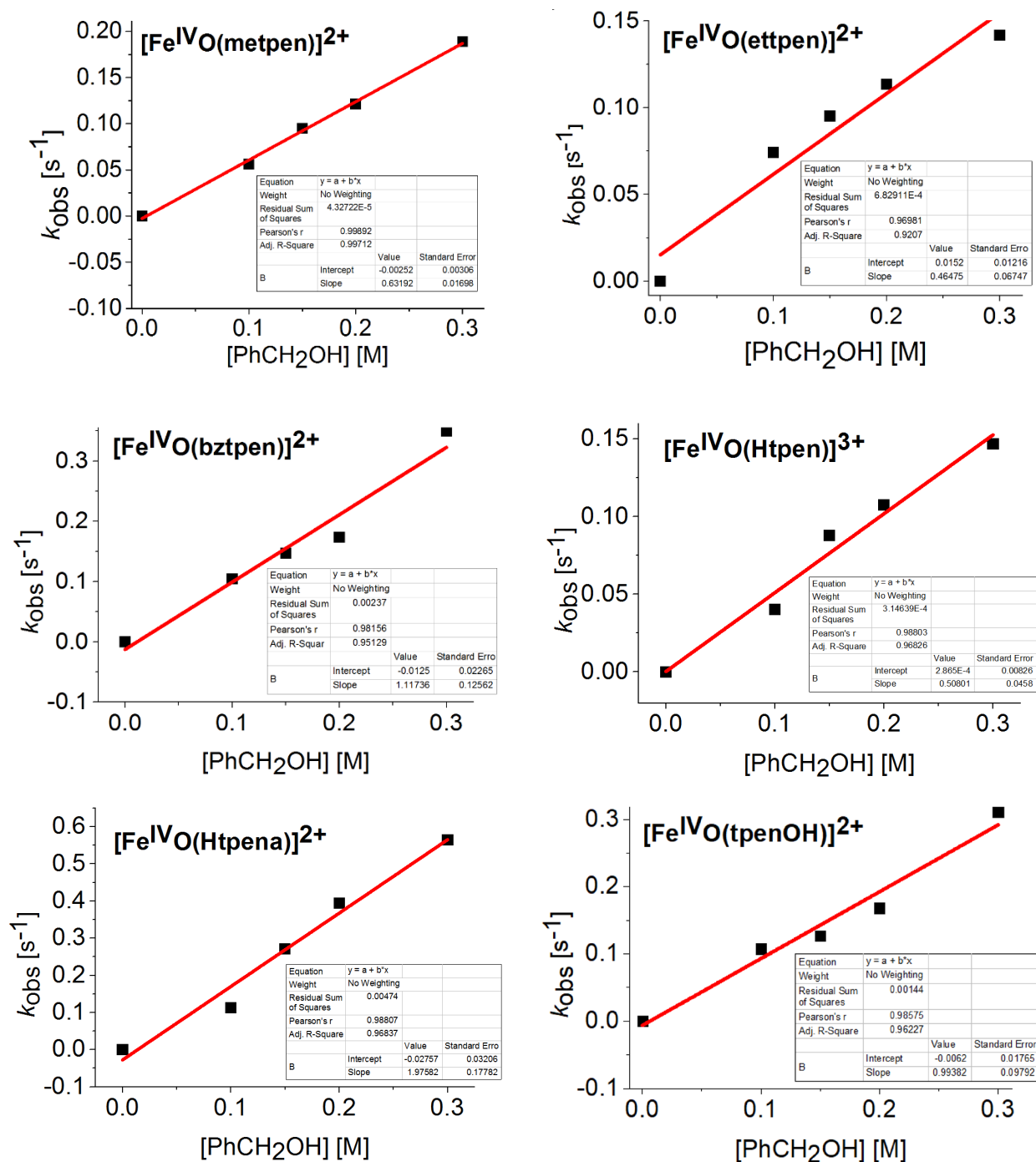


**Figure S4.** Second order rate constant plots ( $k_2$ ) where substrate concentrations of benzyl alcohol is plotted as a function of the pseudo-first-order rate constant,  $k_{obs}$ , for the series of six aqueous iron(IV)oxo species generated from addition of 3. eq. CAN. pH = 2, [Fe] = 1.5 mM, 22 °C. The fitted slopes in red represent  $k_2$ .

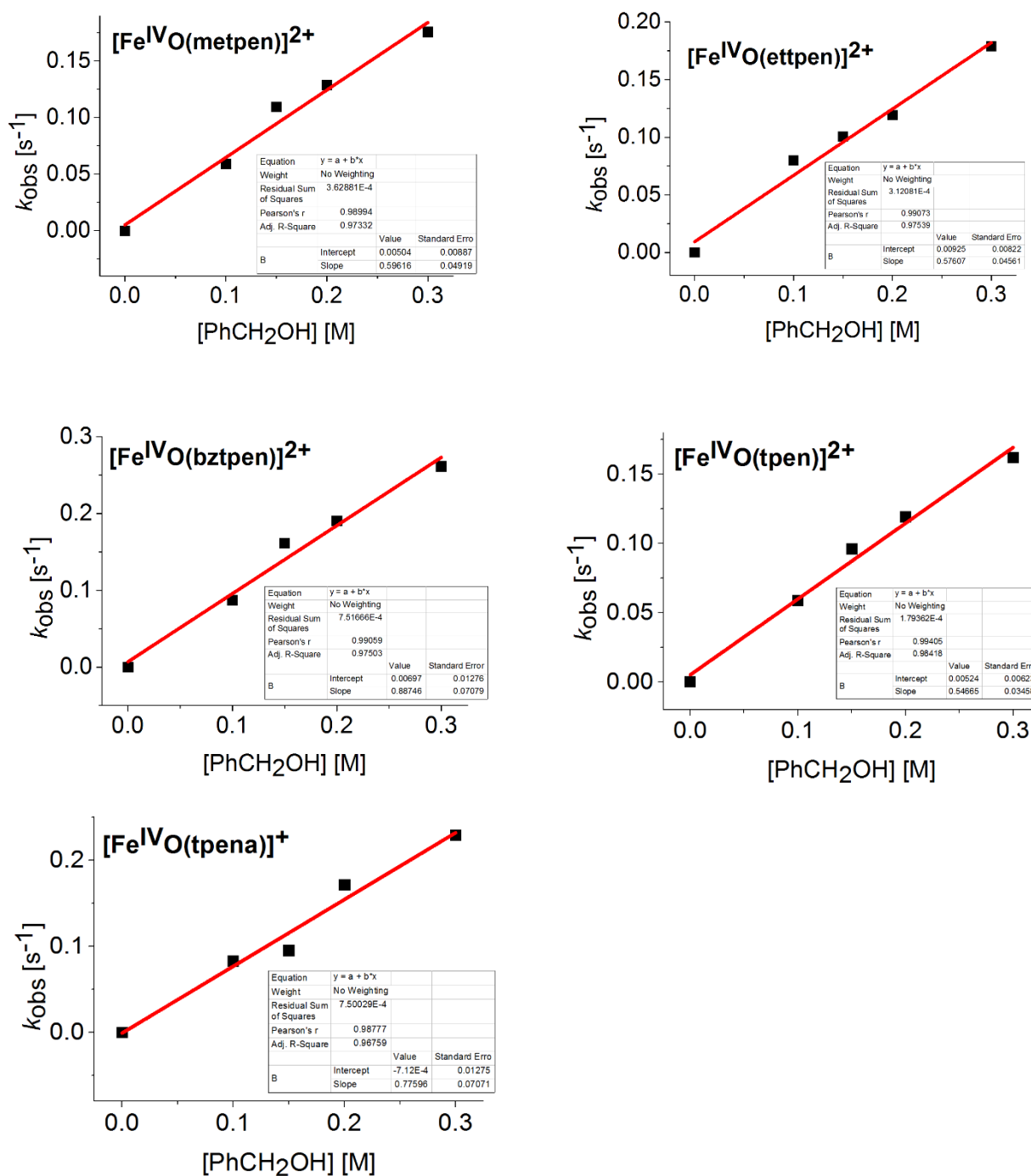


**Figure S5.** Second order rate constant plots ( $k_2$ ) where substrate concentrations of benzyl alcohol is plotted as a function of the pseudo-first-order rate constant,  $k_{\text{obs}}$ , for the series of six aqueous iron(IV)oxo species generated from addition of 3. eq. NaOCl. pH = 7, [Fe] = 1.5 mM, 22 °C. The fitted slopes in red represent  $k_2$ . A  $k_2$  value could not be obtained for [Fe<sup>IV</sup>O(tpenO)]<sup>+</sup> due to the rapid competing intramolecular oxidation of tpenO to tpna under these conditions.

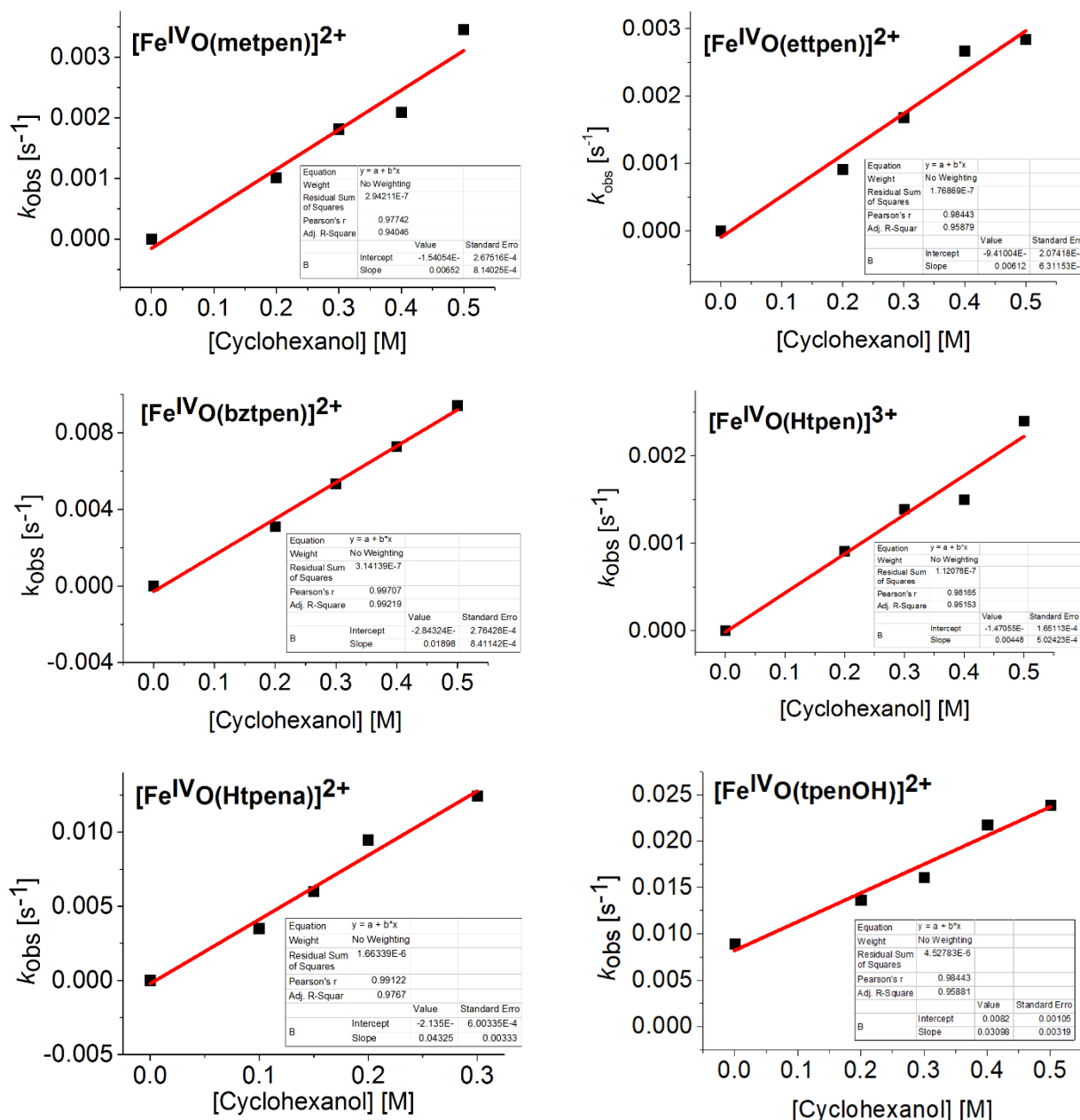


**Figure S6.** Second order rate constant plots ( $k_2$ ) where substrate concentrations of cyclohexanol is plotted as a function of the pseudo-first-order rate constant,  $k_{\text{obs}}$ , for the series of six aqueous iron(IV)oxo species generated from addition of 3. eq. CAN. pH = 2, [Fe] = 1.5 mM, 22 °C. The fitted slopes in red represent  $k_2$ .

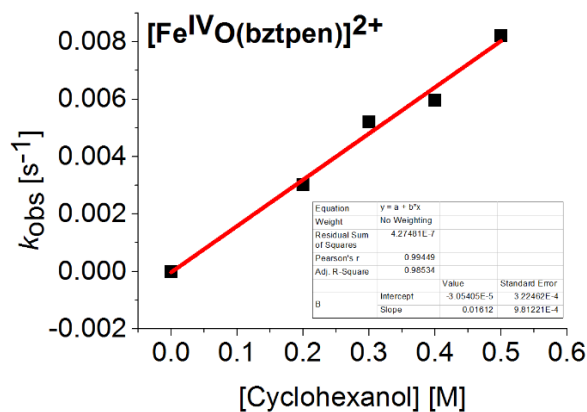
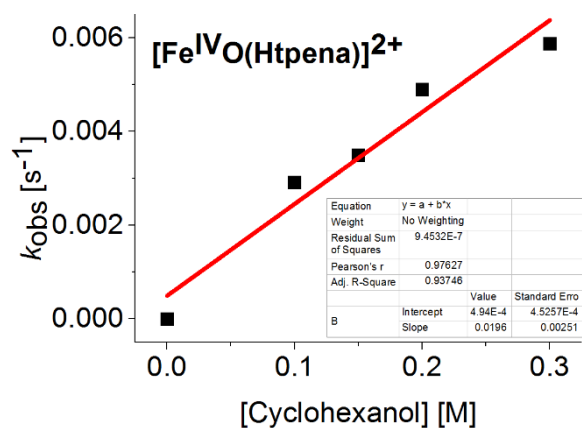


**Figure S7.** Second order rate constant plots ( $k_2$ ) where substrate concentrations of cyclohexanol is plotted as a function of the pseudo-first-order rate constant,  $k_{obs}$ , for [Fe<sup>IV</sup>O(tpena)]<sup>+</sup> and [Fe<sup>IV</sup>O(bztpen)]<sup>2+</sup> generated from addition of 3. eq. NaOCl. pH = 7, [Fe] = 1.5 mM, 22 °C. The fitted slopes in red represent  $k_2$ .

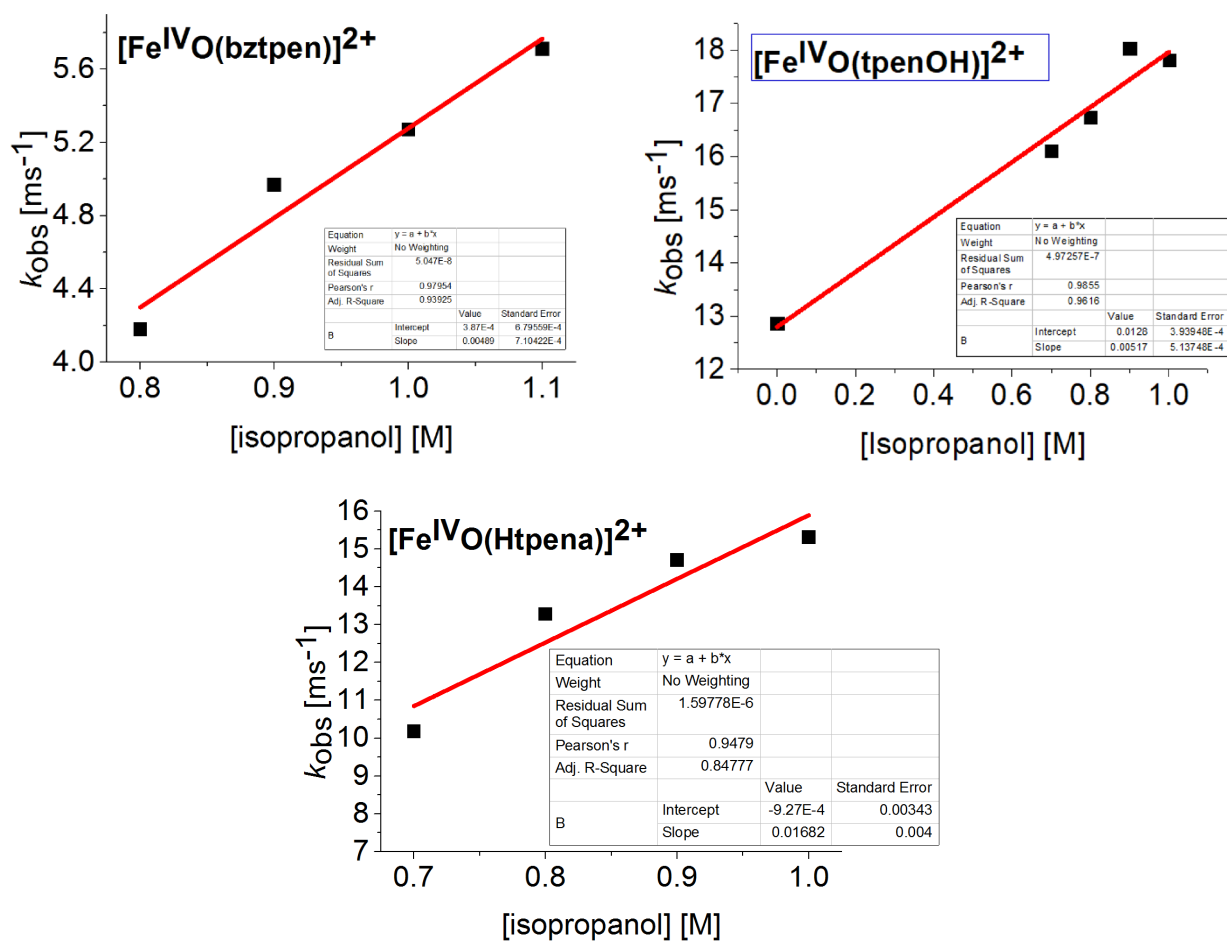


**Figure S8.** Second order rate constant plots ( $k_2$ ) where substrate concentrations of isopropanol is plotted as a function of the pseudo-first-order rate constant,  $k_{obs}$ , for [Fe<sup>IV</sup>O(bztpen)]<sup>2+</sup>, [Fe<sup>IV</sup>O(Htpena)]<sup>2+</sup> and [Fe<sup>IV</sup>O(HtpenO)]<sup>2+</sup> generated from addition of 3. eq. CAN. pH = 2, [Fe] = 1.5 mM, 22 °C. The fitted slopes in red represent  $k_2$ .

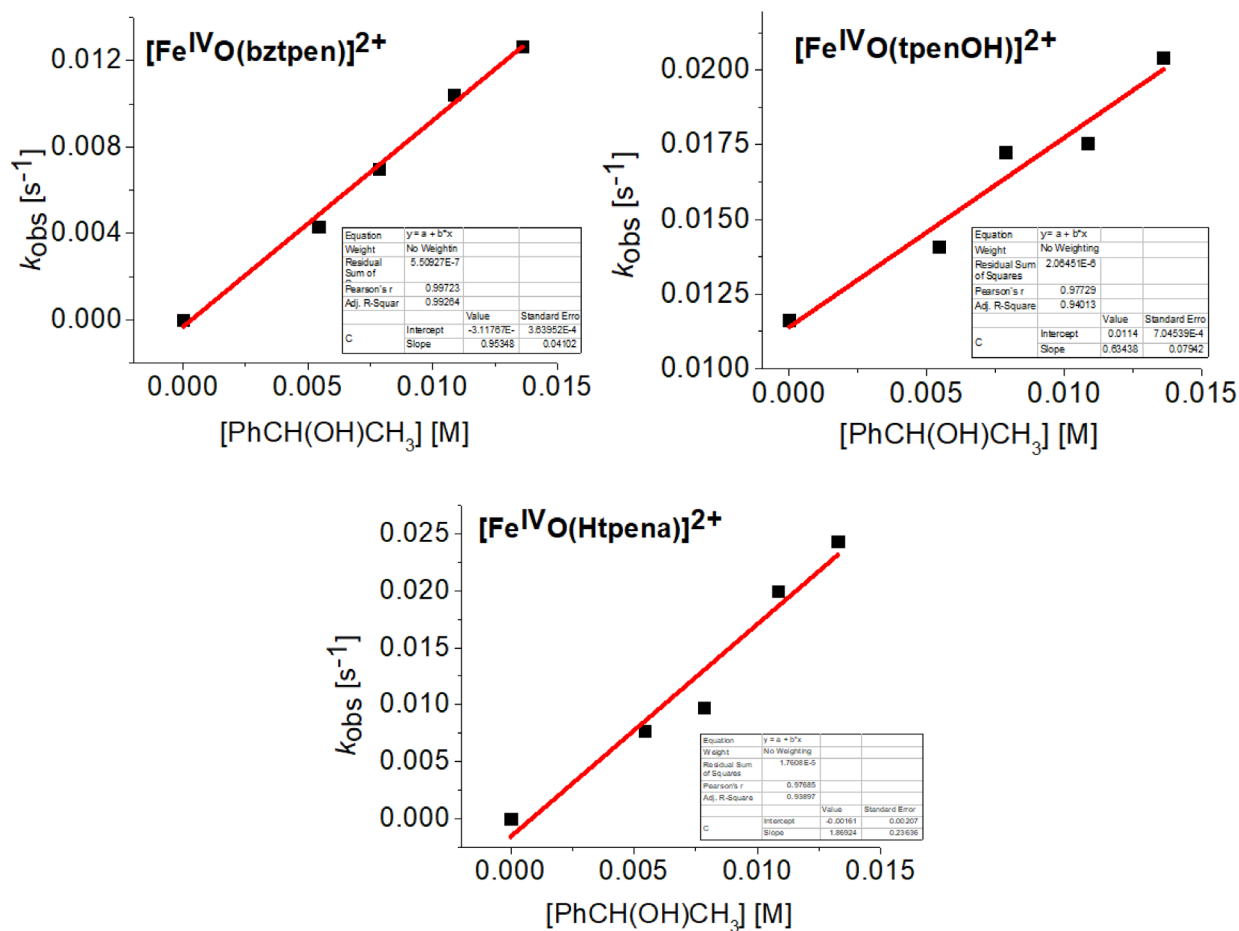


**Figure S9.** Second order rate constant plots ( $k_2$ ) where substrate concentrations of 1-phenylethanol is plotted as a function of the pseudo-first-order rate constant,  $k_{\text{obs}}$ , for  $[\text{Fe}^{\text{IV}}\text{O}(\text{bztpen})]^{2+}$ ,  $[\text{Fe}^{\text{IV}}\text{O}(\text{Htpena})]^{2+}$  and  $[\text{Fe}^{\text{IV}}\text{O}(\text{HtpenO})]^{2+}$  generated from addition of 3. eq. CAN. pH = 2,  $[\text{Fe}] = 0.75 \text{ mM}$ , 22 °C. The fitted slopes in red represent  $k_2$ .



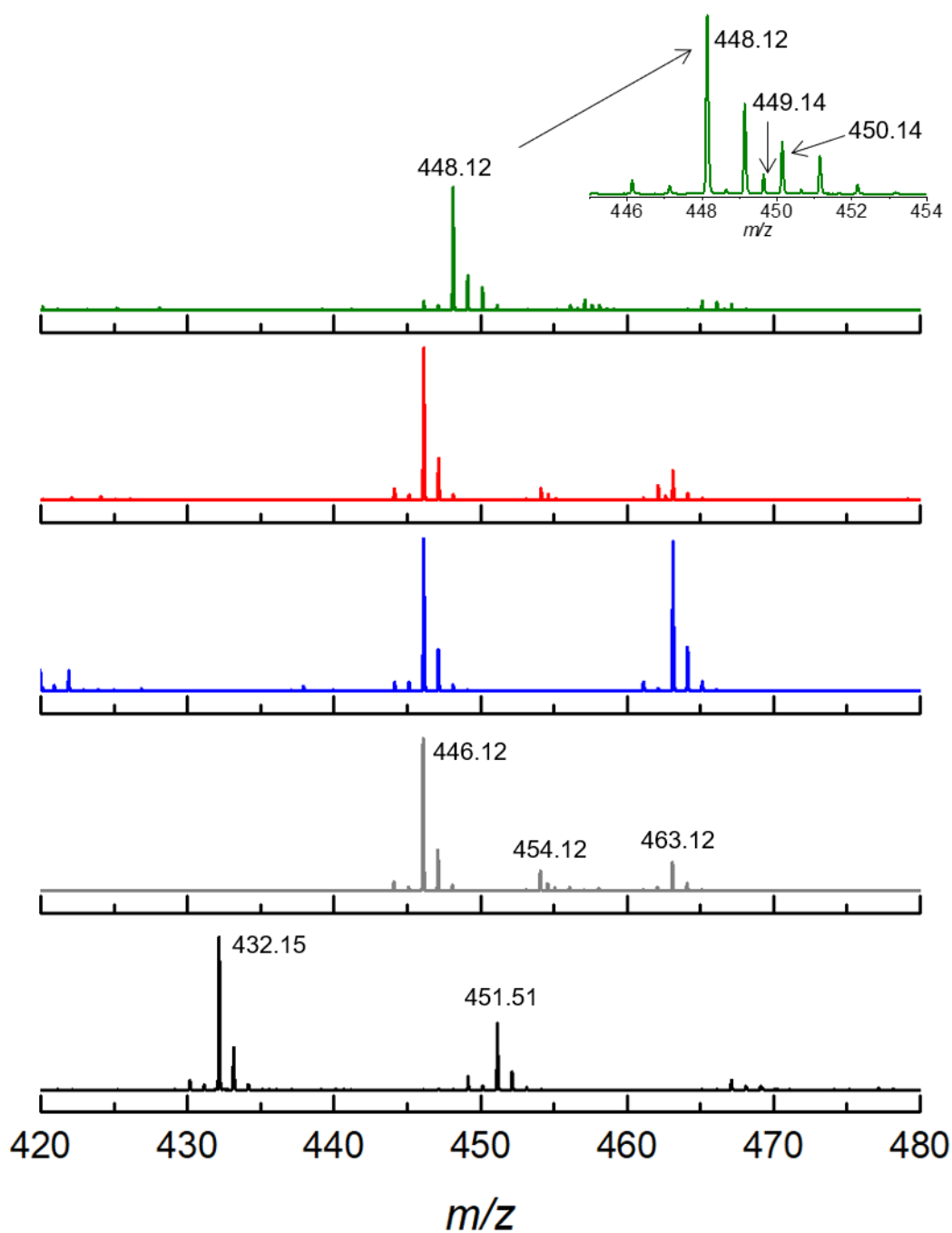


**Figure S10.** ESI-MS spectra of  $[\text{FeCl}(\text{tpenOH})](\text{PF}_6)$  in water (black), and after addition of 6 eq. CAN (blue), 3 eq.  $\text{ClO}^-$  (red) or 3 eq.  $\text{Cl}^{18}\text{O}^-$  (green).  $[\text{Fe}_2\text{O}(\text{tpenAH})_2](\text{ClO}_4)_4$  dissolved in water is shown in grey. Assignments:  $m/z$  463.12,  $[\text{Fe}^{\text{III}}\text{OH}(\text{tpena})]^+$ ; 454.12,  $[\text{Fe}_2^{\text{III}}\text{O}(\text{tpena})_2]^{2+}$ ; 451.15,  $[\text{Fe}^{\text{III}}\text{F}(\text{tpenO})]^+$ ; 448.12,  $^{18}\text{O}-[\text{Fe}^{\text{II}}(\text{tpena})]^+$ ; 446.12,  $[\text{Fe}^{\text{II}}(\text{tpena})]^+$ ; 432.15,  $[\text{Fe}^{\text{II}}(\text{tpenO})]^+$ . Insert: Zoom of  $m/z$  448.12 showing the isotopes  $m/z$  450.14 ( $^{18}\text{O}^{18}\text{O}-[\text{Fe}^{\text{II}}(\text{tpena})]^+$ ) and 449.14 ( $\{^{16}\text{O}-[\text{Fe}^{\text{II}}(\text{tpena})] + ^{18}\text{O}-[\text{Fe}^{\text{II}}(\text{tpena})]\}^{2+}$ ).

## References

- (1) Frisch, M. J.; Trucks, G. W.; Schlegel, H. B.; Scuseria, G. E.; Robb, M. A.; Cheeseman, J. R.; Scalmani, G.; Barone, V.; Petersson, G. A.; Nakatsuji, H.; Li, X.; Caricato, M.; Marenich, A. V.; Bloino, J.; Janesko, B. G.; Gomperts, R.; Mennucci, B.; Hratchian, H. P.; Ortiz, J. V.; Izmaylov, A. F.; Sonnenberg, J. L.; Williams-Young, D.; Ding, F.; Lipparini, F.; Egidi, F.; Goings, J.; Peng, B.; Petrone, A.; Henderson, T.; Ranasinghe, D.; Zakrzewski, V. G.; Gao, J.; Rega, N.; Zheng, G.; Liang, W.; Hada, M.; Ehara, M.; Toyota, K.; Fukuda, R.; Hasegawa, J.; Ishida, M.; Nakajima, T.; Honda, Y.; Kitao, O.; Nakai, H.; Vreven, T.; Throssell, K.; Montgomery, Jr., J. A.; Peralta, J. E.; Ogliaro, F.; Bearpark, M. J.; Heyd, J. J.; Brothers, E. N.; Kudin, K. N.; Staroverov, V. N.; Keith, T. A.; Kobayashi, R.; Normand, J.; Raghavachari, K.; Rendell, A. P.; Burant, J. C.; Iyengar, S. S.; Tomasi, J.; Cossi, M.; Millam, J. M.; Klene, M.; Adamo, C.; Cammi, R.; Ochterski, J. W.; Martin, R. L.; Morokuma, K.; Farkas, O.; Foresman, J. B.; Fox, D. J. *Gaussian 16*; Gaussian, Inc., Wallingford CT, 2016.
- (2) Becke, A. D. Density-functional Thermochemistry. III. The Role of Exact Exchange. *J. Chem. Phys.* **1993**, *98*, 5648.
- (3) Lee, C.; Yang, W.; Parr, R. G. Development of the Colle-Salvetti Correlation-energy Formula into a Functional of the Electron Density. *Phys. Rev. B, Condens. Matter* **1988**, *37*, 785–789.
- (4) Vosko, S. H.; Wilk, L.; Nusair, M. Accurate Spin-dependent Electron Liquid Correlation Energies for Local Spin Density Calculations: a Critical Analysis. *Can J Phys* **1980**, *58*, 1200–1211.
- (5) Tao, J.; Perdew, J. P.; Staroverov, V. N.; Scuseria, G. E. Climbing the Density Functional Ladder: Nonempirical Meta-generalized Gradient Approximation Designed for Molecules and Solids. *Phys. Rev. Lett.* **2003**, *91*, 146401.
- (6) Weigend, F.; Ahlrichs, R. Balanced Basis Sets of Split Valence, Triple Zeta Valence and Quadruple Zeta Valence Quality for H to Rn: Design and Assessment of Accuracy. *Phys. Chem. Chem. Phys.* **2005**, *7*, 3297–3305.
- (7) Weigend, F. Accurate Coulomb-fitting Basis Sets for H to Rn. *Phys. Chem. Chem. Phys.* **2006**, *8*, 1057–1065.
- (8) Tomasi, J.; Mennucci, B.; Cammi, R. Quantum Mechanical Continuum Solvation Models. *Chem. Rev.* **2005**, *105*, 2999–3093.
- (9) Swart, M.; Gruden, M. Spinning Around in Transition-Metal Chemistry. *Acc. Chem. Res.* **2016**, *49*, 2690–2697.

- (10) Vad, M. S.; Lennartson, A.; Nielsen, A.; Harmer, J.; McGrady, J. E.; Frandsen, C.; Mørup, S.; McKenzie, C. J. An Aqueous Non-heme Fe(IV)oxo Complex with a Basic Group in the Second Coordination Sphere. *Chem. Commun.* **2012**, 48, 10880–10882.
- (11) Bernal, I.; Jensen, I. M.; Jensen, K. B.; McKenzie, C. J.; Toftlund, H.; Tuchagues, J.-P. Iron(II ) Complexes of Polydentate Aminopyridyl Ligands and an Exchangeable Sixth Ligand; Reactions with Peroxides. Crystal Structure of  $[\text{FeL}^1 (\text{H}_2 \text{O})][\text{PF}_6]_2 \cdot \text{H}_2 \text{O}$  [ $\text{L}^1 = \text{N}, \text{N}'\text{-bis-(6-methyl-2-pyridylmethyl)-N}, \text{N}'\text{-bis(2-pyridylmethyl)ethane-1,2-diamine}$ ]. *J. Chem. Soc., Dalton Trans.* **1995**, 3667–3675.
- (12) Chang, H. R.; McCusker, J. K.; Toftlund, H.; Wilson, S. R.; Trautwein, A. X.; Winkler, H.; Hendrickson, D. N. [Tetrakis(2-pyridylmethyl)ethylenediamine]iron(II) Perchlorate, the First Rapidly Interconverting Ferrous Spin-crossover Complex. *J. Am. Chem. Soc.* **1990**, 112, 6814–6827.
- (13) Lennartson, A.; McKenzie, C. J. An iron(III) Iodosylbenzene Complex: a Masked Non-heme Fe(V)O. *Angew. Chem. Int. Ed. Engl.* **2012**, 51, 6767–6770.
- (14) Hazell, A.; McKenzie, C. J.; Nielsen, L. P.; Schindler, S.; Weitzer, M. Mononuclear Non-heme Iron(III) Peroxide Complexes: Syntheses, Characterisation, Mass Spectrometric and Kinetic Studies. *J. Chem. Soc., Dalton Trans.* **2002**, 310.
- (15) Jensen, K. B.; McKenzie, C. J.; Nielsen, L. P.; Zacho Pedersen, J.; Svendsen, H. M. Deprotonation of Low-spin Mononuclear iron(III)–hydroperoxide Complexes Give Transient Blue Species Assigned to High-spin iron(III)–peroxide Complexes. *Chem. Commun.* **1999**, 1313–1314.